Calibration of Room Temperature Magnetic Sensor Array for Biomagnetic Measurement

Yoshiaki Adachi[1], Daisuke Oyama[1], Yasushi Terazono[2], Tatsuya Hayashi[2], Tomohiko Shibuya[2], and Shigenori Kawabata[3]

[1]Applied Electronics Laboratory, Kanazawa Institute of Technology, Ishikawa 920-1331, Japan
[2]Advanced Products Development Center, TDK Corporation, Chiba 272-8558, Japan
[3]Department of Advanced Technology in Medicine, Tokyo Medical and Dental University, Tokyo 113-8519, Japan

Biomagnetic field measurement is a promising tool for the investigation of electrical activities in a living body. Room temperature (RT) magnetic sensors with an improved resolution such as magnetoresistance (MR) devices have been recently employed for the detection of weak magnetic fields, which were earlier detected solely using superconducting interference device magnetic sensors. The position, orientation, and sensitivity of each magnetic sensor in a sensor array must be precisely determined for accurate magnetic source analysis. We proposed a calibration method using an array of multiple coils, which is applicable to an RT magnetic sensor array. To demonstrate the validity of the proposed calibration method, we applied it to an MR device-based magnetocardiography (MCG) system equipped with an L-shaped planar sensor array, which was newly developed for the simultaneous observation of both anterior and lateral sides of the body. The deviation of the sensor parameters from the designed values was estimated via calibration. The result of the marker coil localization test indicated that the calibration considerably improved the accuracy of the magnetic source analysis. Finally, we demonstrated a preliminary MCG measurement using the calibrated magnetic sensor array.

Index Terms— **Biomagnetic measurement, calibration, magnetocardiography (MCG) system, magnetoresistance (MR) device.**

I. Introduction

BIOMAGNETIC field measurement is a promising tool for the noninvasive investigation of electrical activities in a living body. The electrical activities of neurons or muscles induce weak magnetic fields that can be detected using highly sensitive magnetic sensors arranged along the body surface. The intensity of the biomagnetic signals is fairly small and ranges only from several femtotesla to several tens of picotesla. Therefore, superconducting quantum interference devices (SQUIDs) have been employed for detecting biomagnetic signals so far [1].

Recently, room temperature (RT) magnetic sensors with an improved resolution such as fluxgate or magnetoresistance (MR) devices have been employed for the detection of weak biomagnetic fields. Magnetocardiography (MCG) performed using RT magnetic sensors has been reported [2], [3]. RT magnetic sensors have a significant advantage over the SQUID magnetic sensors in terms of flexibility in sensor arrangement. As a cryostat is not necessary for RT magnetic sensors in contrast to the SQUID magnetic sensors, RT magnetic sensors can be positioned closer to the magnetic source and larger magnetic signals can be obtained. Furthermore, the RT magnetic sensors can be arranged over a wider observation area because the size of the sensor array is not limited by the size of the cryostat.

Manuscript received October 31, 2018; revised January 5, 2019 and January 21, 2019; accepted January 22, 2019. Date of publication March 5, 2019; date of current version June 20, 2019. Corresponding author: Y. Adachi (e-mail: adachi@ael.kanazawa-it.ac.jp).

Color versions of one or more of the figures in this paper are available online at http://ieeexplore.ieee.org.

Digital Object Identifier 10.1109/TMAG.2019.2895355

The electrical activities of neurons or muscles are reconstructed by applying magnetic source analysis to the magnetic field distribution obtained through the biomagnetic measurements. Functional information is visualized as the transient of reconstructed current distribution around the neurons or muscles superimposed on the anatomical image obtained using magnetic resonance imaging or X-ray computed tomography. For accurate biomagnetic source analysis and superimposition, the position and orientation relative to a subject, and the sensitivity of each magnetic sensor must be precisely determined.

Calibration methods to determine the position, orientation, and sensitivity of SQUID magnetic sensors using an array of multiple coils have already been proposed [4], [5]. In SQUID magnetic sensor arrays, it is necessary to calibrate after cooling because the holder of SQUID magnetic sensors must be non-magnetic and is usually made of plastic, and it inevitably becomes strained at cryogenic temperature. Therefore, the position and orientation of the magnetic sensors are unpredictably shifted from the designed values even if the SQUID magnetic sensor array is manufactured in accordance with the specifications.

In contrast to SQUID magnetic sensors, RT magnetic sensor arrays have no strain at cryogenic temperatures as they are not exposed to such temperature. However, there is non-negligible variation in the performance of the high-sensitivity RT magnetic sensors because they are still in their period of development and the appropriate reproducibility of manufacturing sensors has not been well-established yet. Therefore, the sensitivity calibration of an individual RT magnetic sensor is required for accurate measurements. In particular, for the RT magnetic sensors equipped with a solenoidal pick-up coil or a

flux concentrator of a certain size for sensitivity improvement, it is often difficult to determine the effective sensitivity point and orientation.

In this paper, we propose a calibration method using an array of multiple coils that is applicable to RT magnetic sensor arrays as well as SQUID magnetic sensor arrays and demonstrate that the calibration of the sensor array improves the accuracy of the magnetic source analysis with a newly developed RT-magnetic-sensor-based MCG system.

II. Method

A. Basic Principle of Calibration

An array of coils was prepared to calibrate RT magnetic sensor arrays. The position and orientation of each coil were mechanically determined, and the electric current applied to the coils was calibrated in advance. We applied multiple sets of three-axis concentric circular coils combined into a bobbin [4]. Multiple bobbins could be arranged flexibly to fit into the configuration of the sensor array.

In general, the characteristics of a magnetic sensor are determined by six parameters. Five of them are the three position coordinates (x, y, z) and two sensitivity orientation coordinates (θ, ϕ). The sixth parameter is the sensitivity (g), which represents the conversion coefficient from the magnetic flux density to voltage and its unit is T/V. $B_{\mathrm{cal},j}$, the theoretical magnetic field from the jth circular coil $\mathbf{C}_j$ to be detected by a certain magnetic sensor in the array, is calculated from i_j, the intensity of the current fed to $\mathbf{C}_j$, and is expressed as

$$B_{\mathrm{cal},j} = F(\mathbf{C}_j, i_j | x, y, z, \theta, \phi). \tag{1}$$

In the case of circular coils, F is a function that includes elliptic integrals.

When $B_{\mathrm{meas},j}$, the magnetic field from the jth coil measured by a certain magnetic sensor, is represented as $B_{\mathrm{meas},j} = gV_{\mathrm{meas},j}$, where $V_{\mathrm{meas},j}$ is the signal obtained from the magnetic sensor, the five parameters of the magnetic sensor (x, y, z, θ, and φ) should be determined to obtain the minimum L as follows:

$$L = \sum_j (B_{\mathrm{cal},j} - gV_{\mathrm{meas},j})^2. \tag{2}$$

This is equivalent to minimizing E given as follows:

$$E = 1 - \frac{(\mathbf{B}_{\mathrm{cal}} \cdot \mathbf{V}_{\mathrm{meas}})^2}{|\mathbf{B}_{\mathrm{cal}}|^2 |\mathbf{V}_{\mathrm{meas}}|^2} \tag{3}$$

where $\mathbf{B}_{\mathrm{cal}} = (B_{\mathrm{cal},1}, \ldots, B_{\mathrm{cal},M})$ and $\mathbf{V}_{\mathrm{meas}} = (V_{\mathrm{meas},1}, \ldots, V_{\mathrm{meas},M})$, and the number of coils is denoted by M. To minimize E, parametric optimization based on the Hooke–Jeeves direct search algorithm [6] was applied to determine the best set of the five parameters including the effective position and sensitivity orientation through a numerical search.

After the five parameters were determined, the sensitivity of the magnetic sensor was determined as

$$g = \frac{|\mathbf{B}_{\mathrm{cal}}|^2}{\mathbf{B}_{\mathrm{cal}} \cdot \mathbf{V}_{\mathrm{meas}}}. \tag{4}$$

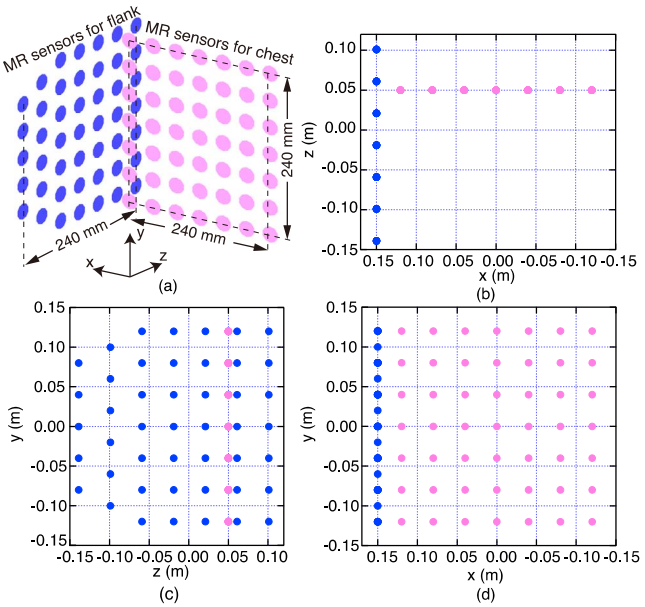

Fig. 1. Design of the L-shaped planar sensor array. (a) Air view of the L-shaped planar sensor array. (b)–(d) Designed positions of magnetic sensors. Pink and blue dots: positions of the MR-device-based magnetic sensors for chest and flank, respectively. The direction of the x-axis in (b) and (d) is from right to left.

B. L-Shaped Planar Sensor Array

The calibrated sensor array had an L-shaped planar configuration designed to collect MCG signals from both chest and flank of sitting subjects as shown in Fig. 1. The array was composed of 95 MR-device-based magnetic sensors (pT-MR sensor, pre-commercial model, TDK, Tokyo, Japan) [7]. Forty-nine of them were arranged in an area of 240 mm × 240 mm at even intervals and oriented in the z-direction to collect the MCG signals from the anterior side of the subject. The remaining 46 magnetic sensors were arranged along the plane perpendicular to the sensor array from the anterior side and oriented in the x-direction to collect the MCG signals from the left lateral side, covering an area of 240 mm × 240 mm. Each magnetic sensor was equipped with flux concentrators and implemented in a plastic case with the outer dimensions of 8 mm × 8 mm × 69 mm together with an amplifier and a bandpass filter of 0.07–200 Hz. The linearity error is less than 0.5% in the range of 10 nT. The output of each magnetic sensor was directly connected to a multichannel digital data acquisition system.

C. Design of Calibration Coil Array

In designing the calibration coil array, the diameter of the circular coil, number of turns, and coil arrangement should be determined by considering the following two points. First, each magnetic sensor could receive the magnetic fields from at least six coils at sufficient signal-to-noise ratio (SNR) because the number of unknown parameters to be determined was six. Second, the coils should not be too close to the magnetic sensors to prevent the output signals from becoming saturated by the large magnetic fields from the coils.

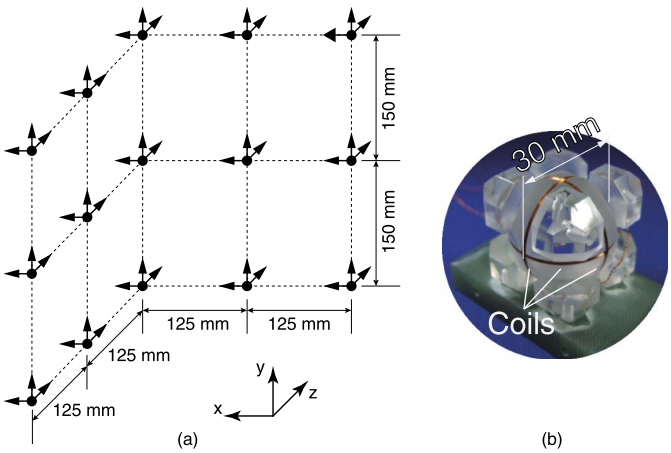

Fig. 2. (a) Arrangement of 15 sets of three-axis concentric coils for the L-shaped planes sensor array. Dots and arrows: positions of the centers and orientations of the coils, respectively. (b) Appearance of a bobbin for three-axis concentric coils.

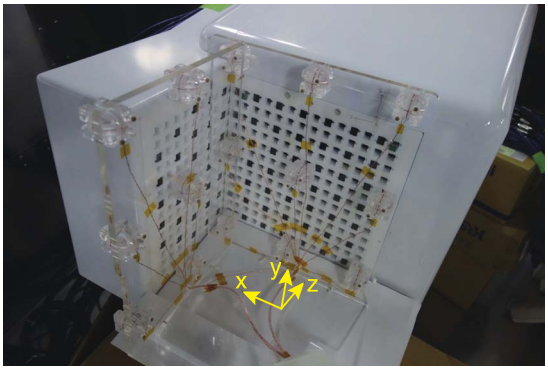

Fig. 3. Calibration coil array set to the L-shaped planar sensor array.

We manufactured the coil array optimized for the calibration of the L-shaped planar MR-device-based magnetic sensor array, considering the aforementioned two points. The 15 sets of the three-axis concentric coils were arranged at the precisely determined positions and orientations as shown in Fig. 2(a). The coil array was configured with 45 coils. A bobbin for the three-axis concentric coils, shown in Fig. 2(b), and the substrate to fix the bobbins was both made of acrylic plastic. The diameter and the number of turns of each coil were 30 and 10 mm, respectively. The mechanical precision of the manufactured coils and assembly was ± 0.1 mm. The minimum distance between the center of the coils and the assumed positions of magnetic sensors was set to approximately 50 mm.

III. Measurements

A. Data Acquisition for Calibration

The coil array was set for the calibration of the L-shaped planar MR-device-based magnetic sensor array as shown in Fig. 3. Sinusoidal tone-burst-like current at the frequency of 80 Hz with the duration of 300 ms was applied to the 45 coils one by one. The intensity of the current was 1.0 mA, and the intensity of the magnetic fields at the sensor array was estimated to be a maximum of approximately 10 nT. The measurements were performed in a magnetically shielded

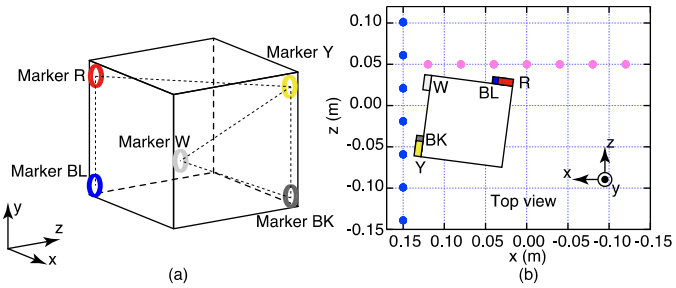

Fig. 4. Setting of marker coils. (a) Five marker coils arranged along the surface of a cube. (b) Position of the cube on which the marker coils were attached.

room (MSR) with the shielding factor of 40 dB at 100 Hz. To avoid the influence of the MSR on the distribution of the magnetic fields generated by the coils, the sensor array and coil array were positioned at a sufficient distance from the wall and floor of the MSR.

Individual magnetic sensors detected the magnetic field generated by each coil separately. The signals from the magnetic sensors were digitally recorded at the sampling rate of 1 kHz, and subsequently averaged 300 times to improve the SNR. The 80 Hz component was extracted from the averaged data using fast Fourier transform (FFT) analysis and was regarded as $V_{\mathrm{meas},j}$. The intensity of the current applied to the coils was simultaneously monitored.

For each magnetic sensor, a numerical search was applied for parametric optimization to determine the best set of the parameters including the effective position, orientation, and sensitivity as described in Section II-A. The effective positions and orientations were first obtained based on the coil array coordination system. These values were transformed to fit the coordination system describing the position of the designed values shown in Fig. 1(b)–(d) using rigid body transformation [8].

The calibration process described earlier was repeated four times and the obtained results were averaged.

B. Marker Coil Measurement

To confirm the effectiveness of the calibration, the magnetic signals from marker coils [9] were recorded using the L-shaped planar MR-device-based magnetic sensor array and the localization of the marker coils was examined. The diameter and the number of turns of the marker coils were 8 mm and 20, respectively. The intensity of the applied current was 2.5–5 mA. Magnetic source analysis was applied to the obtained data, assuming each marker coil to be a magnetic dipole. The positions of the marker coils were estimated under the following three conditions: 1) using the calibrated values for effective positions, orientations, and sensitivities of magnetic sensors; 2) using the calibrated values only for sensitivities and the designed values for positions and orientations of magnetic sensors; and 3) using the designed values for positions, orientations, and sensitivities of magnetic sensors.

Five marker coils indicated by five colors were arranged on the surface of a plastic cube of side 100 mm as shown in Fig. 4(a). The cube was roughly positioned in the region of 0 m $< x <$ 0.15 m and -0.1 m $< z <$ 0.05 m as shown

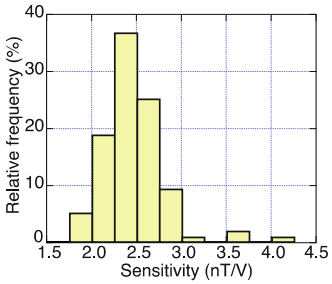

Fig. 5. Histogram of calibrated sensitivities. The number of the sensors is 95.

in Fig. 4(b). This imitated the positioning of a subject in an actual MCG measurement.

The distances between the marker coils represented as dotted lines shown in Fig. 4(a) were precisely measured using a slide caliper with the accuracy of ±0.1 mm in advance and compared with the distances estimated via the magnetic source analysis.

C. Magnetocardiogram Measurement

We performed a preliminary MCG measurement to demonstrate the effectiveness of the calibration under the condition of practical use. The subject was a healthy male in his 30 s. His chest and left flank were tightly contacted to the planar sensor arrays colored in pink and blue in Fig. 1, respectively. The magnetic fields from the body were detected using the MR-device-based magnetic sensors and the magnetic signals from the sensors were continuously recorded digitally, together with the simultaneously detected electrocardiogram (ECG) signals. The sampling rate was 1 kHz, and a bandpass filter of 0.5–200 Hz was applied after the digital recording.

IV. Results and Discussion

A. Results of Calibration

The effective position, orientation, and sensitivity of each magnetic sensor in the L-shaped planar sensor array were individually obtained. The goodness-of-fit (GOF) of the optimization was 99.996% on average. The histogram of sensitivities is shown in Fig. 5. The average sensitivity was 2.44 ± 0.04 nT/V. Even in the MSR, the residual dc magnetic field was still fluctuated due to the neighboring transportation such as railway. To reduce the effect of the dc magnetic field fluctuation, the averaging and extraction of the target signals using FFT were applied, and thereby, the variability of the calibrated sensitivities among the results by the four repeated measurements was suppressed to 0.007 nT/V. It indicated that the effect of the dc magnetic field fluctuation was sufficiently reduced to the negligible level.

Based on the calibrated sensitivity, the noise of each magnetic sensor was estimated. Fig. 6(a) shows a plot of noise spectrum density of a typical magnetic sensor in the sensor array. It is possible that the noise in the lower frequency band could contain the environmental noise as well. The noise level in the white noise region (60–250 Hz) of each sensor, which is corresponding to the magnetic field resolution, was estimated from the noise spectrum density. Fig. 6(b) shows the histogram

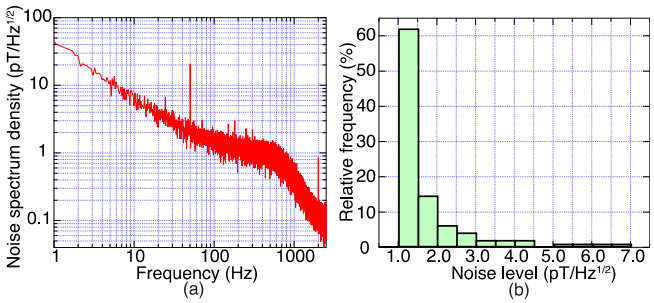

Fig. 6. (a) Noise spectrum density of a typical magnetic sensor in the L-shaped planar sensor array. (b) Histogram of the white noise level of magnetic sensors. The number of sensors is 95.

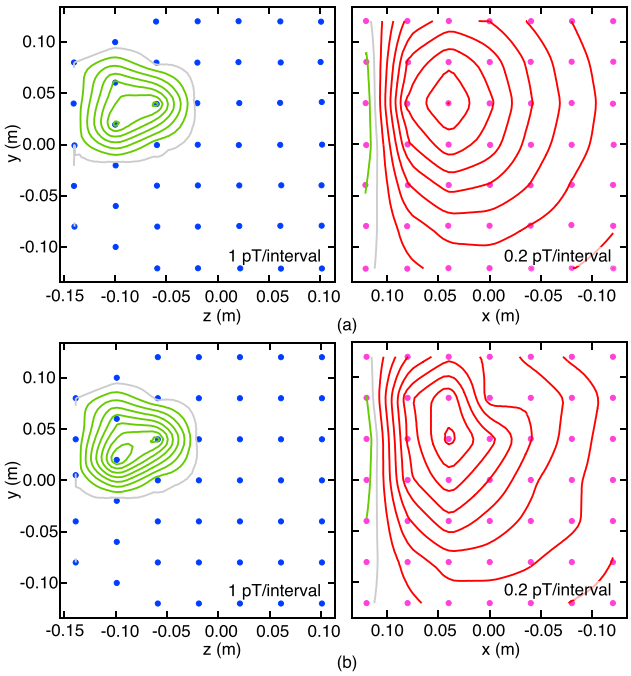

Fig. 7. (a) Example of magnetic field distribution from a marker coil observed by the calibrated sensor array. (b) Apparent magnetic field distribution from the same marker coil assuming that the sensor array was not calibrated.

of the white noise level of magnetic sensors. The noise level of most magnetic sensors was less than 3.0 pT/Hz$^{1/2}$ as shown in Fig. 6(b).

When the planes are fitted to the sensor arrays for both the anterior side and the lateral side separately, the root mean squares of the distances between each magnetic sensor and the fitted planes were 0.6 and 0.9 mm, respectively. The angle between the normal vectors of the two planes was calculated as 90.40°. Regarding the orientation of the magnetic sensors, the averaged shifts from the designed values and their standard deviation were 1.26° and 0.75°, respectively. These parameters indicate that the deviations from the designed values. We could estimate the deviations accurately via calibration.

B. Marker Coil Localization

Fig. 7(a) shows an example of the magnetic field distribution from a marker coil (Marker Y) observed by the calibrated sensor array. When it was assumed that the sensor array was not calibrated and the constant sensitivity (2.5 nT/V) was equally assigned to every magnetic sensor for converting

TABLE I
GOF OF MARKER COIL LOCALIZATION

	Calibrated	Uncalibrated
Marker R	99.989%±0.005%	99.270%±0.699%
Marker Y	99.991%±0.002%	98.777%±0.216%
Marker BL	99.968%±0.018%	99.922%±0.025%
Marker W	99.991%±0.003%	99.457%±0.098%
Marker BK	99.968%±0.011%	99.800%±0.048%

The GOF values are the averaged one with standard deviations of the six trial results obtained at various cube positions.

TABLE II
DISTANCES BETWEEN MARKER COILS

	Measured distance	Estimated (1)	Estimated (2)	Estimated (3)
Marker R–BL	82.2	82.3±0.3 (0.1)	81.6±0.3 (0.5)	83.1±1.0 (1.0)
Marker Y–W	84.1	83.7±0.2 (0.4)	83.5±0.1 (0.6)	83.1±1.3 (1.0)
Marker BK–W	92.9	92.7±0.4 (0.2)	92.6±0.1 (0.3)	94.2±0.8 (1.3)
Marker R–Y	130.1	130.3±0.1 (0.3)	129.2±0.4 (0.9)	131.9±5.8 (1.9)

The conditions (1), (2), and (3) for estimated distances are described in Section III-B. The parenthetic values indicate the deviation from the measured values. All values are in mm.

the voltages to magnetic fields, the contour maps shown in Fig. 7(a) changed to the magnetic field distribution shown in Fig. 7(b). In contrast to Fig. 7(a), the obvious distortion in the distribution was found in Fig. 7(b). Between two sets of the contour maps, the data set itself was identical but only the sensitivity values assigned to each magnetic sensor were different. Therefore, this distortion was considered to originated from the uncalibrated sensitivity. Table I lists the GOF of the localization of each marker coil, which indicated how much the observed magnetic field distribution fitted to the theoretical model of the magnetic field from the marker coil. If the sensor array was not calibrated, the GOFs were inferior to the calibrated ones. These results indicated that the calibration effectively suppressed the distortion of the magnetic field distribution and improved the GOF.

The comparison of the distances between marker coils measured using a slide caliper and estimated via the magnetic source analysis is given in Table II. The estimated values were the averaged ones with standard deviations of the six trial results obtained at various cube positions.

According to Table II, the difference between the measured and estimated values was minimized when the positions, orientations, and sensitivities of the magnetic sensors were calibrated. If the sensor array was not calibrated and the designed values were used for the localization of the marker coils, the errors in the estimated distances would be 1.0 mm or more. It indicated that the marker coil localization accuracy was improved by the calibration. Even if only the sensitivities were calibrated and the designed values were used for the positions and orientations, the estimation accuracy would improve partially.

C. Magnetocardiogram Measurement

Fig. 8 shows the result of the MCG measurement. The waveforms shown in Fig. 8(a) and (b) were obtained via signal averaging of 200 beats. In Fig. 8(a), the magnetic

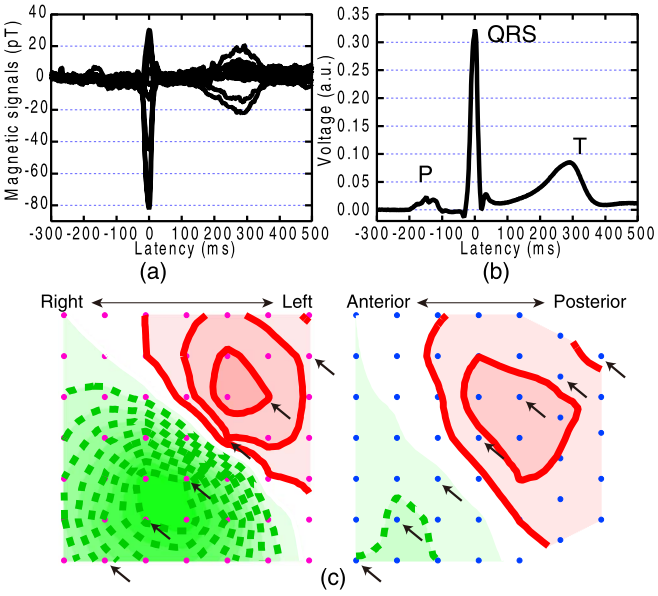

Fig. 8. Result of the MCG measurement. (a) Overlapping waveforms of the magnetic signals obtained from the magnetic sensors marked by arrows in (c). (b) Waveform of the ECG signals recorded simultaneously. (c) Isofield contour map at the R-peak. Red solid and green dotted lines: outward and inward magnetic fields, respectively. The interval between lines is 10 pT.

field components corresponding to the P, QRS, and T-waves identified on the simultaneously recorded ECG waveform shown in Fig. 8(b) can be observed although the signal quality was much worse compared to the one obtained by SQUID magnetic sensors. Fig. 8(c) shows the obtained magnetic distribution over the sensor array at the latency corresponding to the R-peak. This distribution pattern observed by the front sensor array was in a good agreement with the one obtained in our previous study using a magnetic sensor array calibrated by a conventional coil array arranged in a single plane [3].

V. CONCLUSION

In this paper, we proposed a method for the calibration of RT magnetic sensor arrays to obtain the effective position, orientation, and sensitivity of each magnetic sensor using an array of multiple coils and parameter optimization via a numerical search. Although the values obtained from the sensor array deviate from the designed values, if the deviation can be estimated precisely via the calibration, it does not affect the accuracy of the magnetic source analysis.

In contrast to the SQUID magnetic sensors, the MR-device-based magnetic sensors have lesser magnetic field resolution but possess significant flexibility in sensor arrangement. The proposed calibration method can be applied to RT magnetic sensor arrays of any shape by appropriately arranging the three-axis coils as demonstrated herein.

There are several causes of uncertainty in the calibration such as the SNR of measurements, the instability of current source, processing accuracy of coils, and exactness of the computational model. In the L-shaped planar sensor array with the 40 mm sensor intervals, no inter-sensor crosstalk beyond the measurement limit was observed. However, as the distance between the sensors becomes smaller, the crosstalk may affect the uncertainty of the calibration. Although the uncertainty

of the calibration was not discussed in this paper, it is necessary to examine and evaluate these causes of uncertainty in calibration, which will be the subject of our future study.

ACKNOWLEDGMENT

This work was supported in part by KAKENHI, JSPS, Japan under Grant 18K12044. The authors would like to thank Editage (www.editage.jp) for English language editing. They would also like to thank Y. Oshida for her artisanal works for the manufacture of the calibration coils used in this paper.

REFERENCES

[1] R. L. Fagaly, "Superconducting quantum interference device instruments and applications," *Rev. Sci. Instrum.*, vol. 77, no. 10, 2006, Art. no. 101101.

[2] H. Karo and I. Sasada, "Magnetocardiogram measured by fundamental mode orthogonal fluxgate array," *J. Appl. Phys.*, vol. 117, no. 17, 2015, Art. no. 17B322.

[3] Y. Shirai *et al.*, "Magnetocardiography using a magnetoresistive sensor array," *Heart J.*, vol. 60, no. 1, pp. 50–54, 2019. doi: 10.1536/ihj.18-002.

[4] T. Yoshida, M. Higuchi, T. Komuro, and H. Kado, "Calibration system for a multichannel SQUID magnetometer," in *Proc. 16th Annu. Int. Conf. IEEE Eng. Adv., New Opportunities Biomed. Eng.*, Nov. 1994, pp. 171–172.

[5] Y. Adachi, M. Higuchi, D. Oyama, Y. Haruta, S. Kawabata, and G. Uehara, "Calibration for a multichannel magnetic sensor array of a magnetospinography system," *IEEE Trans. Magn.*, vol. 50, no. 11, Nov. 2014, Art. no. 5001304.

[6] R. Hooke and T. A. Jeeves, "'Direct search' solution of numerical and statistical problems," *J. Assoc. Comput. Machinery*, vol. 8, no. 2, pp. 212–229, 1961.

[7] *Capable of Detecting Extremely Weak Biomagnetic Signals at Room Temperature*. Accessed: Aug. 27, 2018. [Online]. Available: https://product.tdk.com/info/en/techlibrary/developing/bio-sensor/index.html

[8] J. H. Challis, "A procedure for determining rigid body transformation parameters," *J. Biomech.*, vol. 28, no. 6, pp. 733–737, 1995.

[9] S. N. Erné, L. Narici, V. Pizzella, and G. L. Romani, "The positioning problem in biomagnetic measurements: A solution for arrays of superconducting sensors," *IEEE Trans. Magn.*, vol. MAG-23, no. 2, pp. 1319–1322, Mar. 1987.